Amyloid Fibril Formation of the Mouse V_L Domain at Acidic pH

Sergey P. Martsev,*,‡ Anatoly P. Dubnovitsky,‡ Alexander P. Vlasov,‡ Masaru Hoshino,§ Kazuhiro Hasegawa,|| Hironobu Naiki,|| and Yuji Goto§

Institute of Bio-Organic Chemistry, National Academy of Sciences of Belarus, Minsk 220141, Belarus, Institute for Protein Research, Osaka University, Yamadaoka 3-2, Suita, Osaka 565-0871, Japan, and Department of Pathology, Fukui Medical University, Matsuoka, Fukui 910-1193, Japan

Received October 26, 2001; Revised Manuscript Received December 26, 2001

ABSTRACT: The recombinant V_L domain that represents the variable part of the light chain (type κ) of mouse monoclonal antibody F11 directed against human spleen ferritin was found to form amyloid fibrils at acidic pH as evidenced by electron microscopy, thioflavin T binding, and apple-green birefringence after Congo red staining. This is the first demonstration of amyloid fibril formation of the mouse V_L domain. To understand the mechanism of acidic pH-induced amyloid fibril formation, conformational changes of the V_L domain were studied by one-dimensional NMR, differential scanning calorimetry, analytical ultracentrifugation, hydrophobic dye binding, far-UV circular dichroism, and tryptophan fluorescence. The results indicated accumulation of two intermediate states during acid unfolding, which might be responsible for amyloid fibril formation. The more structured intermediate that exhibited maximal accumulation at pH 3 retained the nativelike secondary structure and a hydrophobic core, but exposed hydrophobic surfaces that bind 8-anilino-1-naphthalenesulfonate. Below pH 2, a more disordered intermediate with dequenched tryptophan fluorescence but still retaining the β-sheet structure accumulated. The optimal pH of amyloid fibril formation (i.e., pH 4) was close to the optimal pH of the accumulation of the nativelike intermediate, suggesting that the amyloid fibrils might be formed through this intermediate.

Antibody light chain-related (AL)[1] amyloidosis is a pathological process in which the N-terminal fragment of the light chain, including the V_L domain, undergoes self-assembly into highly ordered fibrillar aggregates that are deposited in body tissues. One of the factors that contributes to the disease was shown to be the high level of circulating light chains produced by myeloma or other pathological conditions. However, only ~15% of myeloma patients developed amyloid deposits that may be in the form of either ordered fibrils (AL) or more amorphous, dense granular bodies [light chain deposition disease (LCDD)] (*1*).

Additional features that contribute to formation of amyloid fibrils were analyzed in stability studies using a series of amyloidogenic and nonamyloidogenic recombinant V_L domains from humans (*2*−*6*). The V_L fragment of an amyloidogenic Bence Jones protein was shown to produce amyloid fibrils only at acidic pH, while remaining aggregated, but was not fibrillar at physiological pH (*7*). Fink and co-workers (*8*) applied atomic force microscopy in the study of fibrillogenesis for the amyloidogenic human V_L domain SMA and found that acidic pH increased the rate of in vitro fibril formation and produced a regular form of fibrils. They further examined the relationship between conformation and amyloid fibril formation (*6*) and showed that, while a relatively nativelike intermediate observed between pH 4 and 6 preferentially leads to amorphous aggregates, the more disordered intermediate at pH <3 readily forms amyloid fibrils. These results supported the hypothesis that amyloid fibril formation involves the ordered self-assembly of partially folded species.

Destabilization by low pH was previously shown to produce amyloidogenic intermediates for transthyretin (*9*, *10*) and β2-microglobulin (*11*−*13*). Participation of partly folded intermediates was also indicated in amyloid fibrillogenesis of human lysozyme (*14*). These studies with various proteins other than V_L domains also indicated that it is a decrease in thermodynamic stability rather than sequence-specific features that constitutes another critical determinant of amyloid fibril formation. In support of the presumed role of partially structured amyloidogenic intermediates, Raffen et al. (*5*) demonstrated that nonamyloidogenic human V_L domain LEN was capable of producing amyloid fibrils under conditions of destabilization by moderate GdnHCl concentrations. Experimental evidence in support of the hypothesis that amyloid fibril formation involves the ordered self-assembly of partially folded species is being increasingly accumulated for various amyloidogenic proteins.

Although AL amyloidosis has been studied with various human V_L domains and light chains (Bence Jones proteins), mouse V_L domains have not been considered. Solomon et

* To whom correspondence should be addressed. Telephone: +375 172 637 188. Fax: +375 172 635 128. E-mail: martsev@iboch.bas-net.by.

‡ National Academy of Sciences of Belarus.

§ Osaka University.

|| Fukui Medical University.

[1] Abbreviations: AL, antibody light chain-related; ANS, 8-anilino-1-naphthalenesulfonic acid; CD, circular dichroism; C_H, antibody heavy chain constant domain; C_L, antibody light chain constant domain; DSC, differential scanning calorimetry; Fab, antigen-binding fragment; GdnHCl, guanidine hydrochloride; K_a, association constant; LCDD, light antibody chain deposition disease; NMR, nuclear magnetic resonance; V_L, light chain variable domain; Δh, specific calorimetric enthalpy of unfolding; T_m, midpoint temperature of thermal transition.

10.1021/bi015894u CCC: $22.00
Published on Web 01/30/2002

al. (*15*) reported the successful experimental induction of human AL amyloid deposition in mice by repeated injection of Bence Jones proteins obtained from two patients with AL amyloidosis. However, it is generally thought that mouse light chains do not produce amyloid fibrillar deposits in vivo. In the study presented here, we provide the first description of amyloid fibril formation of the mouse V_L domain. While nonamyloidogenic at physiological pH, the V_L domain formed amyloid fibrils under conditions of low pH through probably either of the two partially unfolded states. These results with the mouse V_L domain further confirmed the critical role of the destabilized conformation for amyloid fibril formation.

MATERIALS AND METHODS

Proteins. Expression and purification of the mouse V_L domain were performed as described previously (*16*, *17*). This recombinant V_L domain (115 amino acids, ~12.8 kDa) represents the variable N-terminal part of the light chain (type κ) of mouse monoclonal antibody F11 directed against human spleen ferritin. The V_L domain was functional with a ferritin binding constant of $\sim 2 \times 10^7$ M^{-1} (*17*), which is ~30 times lower than the ferritin binding constant of the full-length "parent" antibody (*18*, *19*). The purity of the protein was at least 95% as determined by SDS−PAGE. After expression, purification, and refolding from the denaturants (GdnHCl or urea), the protein was concentrated and stored in 0.02 M sodium phosphate buffer (pH 8.0). The protein was typically used for further experiments within 5 days.

Thioflavin T Binding Studies. The final V_L concentration in the thioflavin T binding assay varied between 0.7 and 1.2 mg/mL. For the standard measurements, the concentration of 1 mg/mL (~82 μM) was used. A composite buffer containing 25 mM sodium acetate and 25 mM sodium phosphate was used in the pH range of 1.5−7.5. In the low-pH region, the pH was adjusted with HCl, and above pH 5.5, NaOH was used for titration up to the required pH. Sodium chloride was added to adjust the ionic strength to a fixed value of 0.2 at each pH. Before incubation, each sample with the V_L domain solution (3−5 mg/mL) was passed through a 0.2 μm filter to remove traces of aggregated material. From 0.6 to 1.0 mL of the reaction mixture was then incubated at 37 °C with agitation at 100−150 rpm in capped glass tubes (12 mm × 70 mm) fixed obliquely on a shaking plate. To obtain a time course curve, aliquots of 10 μL were removed after 2, 3, 6, and 11 days and added to 1 mL of a thioflavin T solution (final concentration of 10 μM) at pH 8.5 in 100 mM sodium borate buffer. Emission spectra were monitored with excitation at 450 nm using either a Hitachi F-4500 or SFL-1211 (Solar) spectrofluorometer. The emission intensity of bound thioflavin T was measured at 485 nm. Control experiments showed that the fibrils formed at low pH were stable at pH 7.0−8.5 over the time course of the measurements. The fluorescence of thioflavin T alone was also measured at each pH, and the emission intensity was subtracted from that determined in the presence of both the protein and thioflavin T.

CD Measurements. CD spectra were recorded with a J-520 spectropolarimeter (Jasco) at protein concentrations of 0.5−0.8 mg/mL in a thermostatically controlled cuvette holder using a 1 mm quartz cell for the far-UV spectra. Spectra were usually recorded from 200 to 250 nm at a scan speed of 5 or 10 nm/min. The averaged spectra of several scans were corrected relative to the buffer blank. Mean residue ellipticities were calculated using a value of 115 for the mean residue molecular weight.

Fluorescence Measurements. Fluorescence spectra of the proteins and protein−ANS complexes were recorded at room temperature and a protein concentration of 0.1 mg/mL in a 1 cm path length cuvette using either a Hitachi F-4500 or SFL-1211 (Solar) fluorometer as described by Martsev et al. (*16*). The protein intrinsic fluorescence was measured with excitation at 280 nm, and the ANS fluorescence was measured with excitation at 360 nm. The ANS:protein molar ratio was 10:1.

Differential Scanning Calorimetry. Measurements were performed with a DASM-4 scanning calorimeter (Biopribor, Pushchino, Russia) in the temperature range of 10−100 °C at a scan speed of 60 K/h. In all experiments, the reference cell was filled with the buffer used to dialyze the protein sample. Unless otherwise specified, the buffers used for the calorimetric measurements were as follows: 0.05 M sodium phosphate-HCl at pH 2.0, 0.05 M phosphate-citrate at pH 3.0, and 0.05 M sodium phosphate at pH 5.0 and 7.0. The instrumental baseline was subtracted from the heat capacity curves that were obtained. The baseline was determined prior to each protein scan with both cells filled with the buffer. The protein concentrations in calorimetric experiments ranged between 1 and 2.5 mg/mL. Three to four scans were recorded for each sample, with variations of enthalpy measurements being within the range of 5−7%. The calorimetric enthalpy was calculated according to the method of Privalov and Khechinashvili (*20*). Heat capacity curves were analyzed and deconvoluted using WSCAL and TERMCALC software based on the method described by Privalov and Potekhin (*21*). The software was supplied by the DASM-4 manufacturer.

Analytical Ultracentrifugation. Sedimentation equilibrium experiments were performed with a Beckman Optima XL-A analytical ultracentrifuge at 20 000 rpm. The measurements at various pH values were performed at 20 °C. Samples were dialyzed against the buffer at the required pH and analyzed at concentrations of 0.15 and 0.45 mg/mL (11.7 and 35.1 μM, respectively) for pH 3.95 and at 0.45 mg/mL for pH 8 and 2.35. The data were obtained after centrifugation for 20 h by monitoring the absorbance at 278 nm. For the V_L domain having a molecular mass of 12 824 Da, a partial specific volume of 0.727 mL/g (25 °C) was obtained as described by Laue et al. (*22*). Concentration versus radius data were acquired with an average of 20 absorbance measurements over 0.001 cm intervals. All experiments used double-sector 12 mm thick charcoal-epon centerpieces and matched quartz windows. The protein concentration (C_T) was plotted against radius (r) from the arbitrary radius point. The C_T versus r plots were analyzed to determine the dimerization/association constant (K_a) according to the theoretical equation for monomer−dimer equilibrium as described elsewhere (*23*, *24*) with the least-squares curve fitting using IGOR software (WaveMetrics, Lake Oswego, OR).

NMR. One-dimensional ^{1}H NMR spectra were recorded on a 500 MHz spectrometer (Bruker DMX 500) equipped with a triple-axis-gradient triple-resonance probe. The spectral width was 8012.8 Hz, and 128 scans of 4096 real time

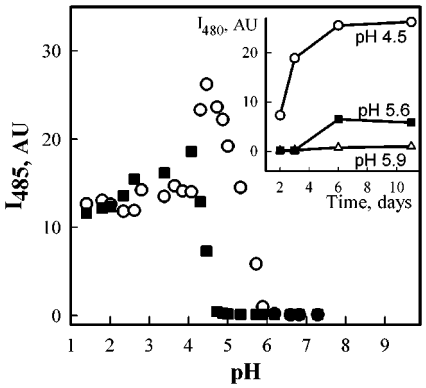

FIGURE 1: pH dependence of thioflavin T fluorescence after incubation with the V_L domain for 3 (■) and 11 days (○) at 37 °C. The inset shows the time course of changes in thioflavin T fluorescence at pH 4.5, 5.6, and 5.9.

points were collected for 3 min. The protein concentration was 2.0 mg/mL, and the temperature was 20 °C.

Electron Microscopy. To obtain the electron micrographs, reaction mixtures were spread on carbon-coated grids, negatively stained with 1% phosphotungstic acid (pH 7.0), and examined with a Hitachi H-7000 electron microscope with an acceleration voltage of 75 kV.

Other Methods. A part of the reaction mixture was spread on glass slides, dried overnight in an incubator set at 37 °C, stained with Congo red, and examined under a polarized light microscope to check for apple-green birefringence. SDS−PAGE was performed according to the method of Laemmli (*25*) and stained with Coomassie Brilliant Blue R-250. The concentration of the V_L domain was determined from the absorption of a 0.1% solution in a 1 cm path length cuvette at 280 nm. The absorption value of 1.15 was calculated from the amino acid sequence according to the method of Gill and von Hippel (*26*).

RESULTS

Amyloid Fibril Formation. Amyloid fibril formation was monitored using a fluorescence assay that employs the known propensity of the dye thioflavin T to enhance the emission intensity and to shift the emission wavelength on binding to amyloid fibrils (*27*). At pH 4.5, the V_L domain produced thioflavin T binding species that became evident after incubation for 3 days at 37 °C (Figure 1). More acidic conditions were slightly less efficient with regard to the formation of insoluble thioflavin T binding species. More prolonged incubation resulted in the less acidic pH required for the onset of the process. After 11 days at 37 °C, a small but reliably detected thioflavin T fluorescence was observed at pH 5.6 but not at pH 5.9. It is noteworthy that even after a 60 day incubation at physiological pH and 37 °C, the V_L domain did not reveal binding of thioflavin T.

Thioflavin T binding species were unambiguously identified as amyloid fibrils with two additional methods. First, Congo red staining resulted in apple-green birefringence when viewed under cross-polarized light (data not shown). Second, straight fibrils with a diameter of ~10 nm (Figure 2) formed at pH 3.0−3.8 were similar to human AL amyloid fibrils. These results confirmed that the mouse V_L domain formed typical amyloid fibrils.

Analytical Ultracentrifugation. To obtain insight into the mechanism of amyloid formation, we characterized the pH-dependent conformational change of the mouse V_L domain with various methods. First, analytical ultracentrifugation (Figure 3) showed the pH-dependent shift of a monomer−dimer equilibrium, as described previously for human V_L

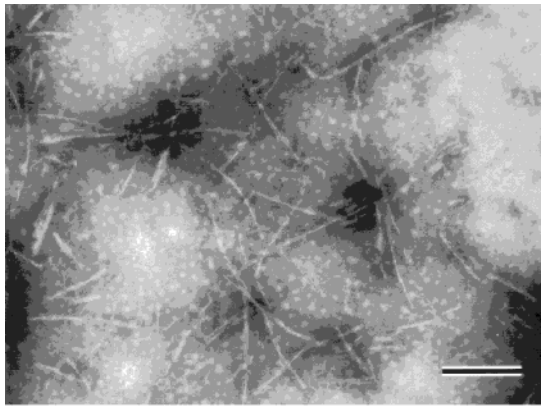

FIGURE 2: Electron micrograph of amyloid fibrils produced by incubation of the V_L domain (1.0 mg/mL) at pH 3.0 and 37 °C. The scale bar is 250 nm in length.

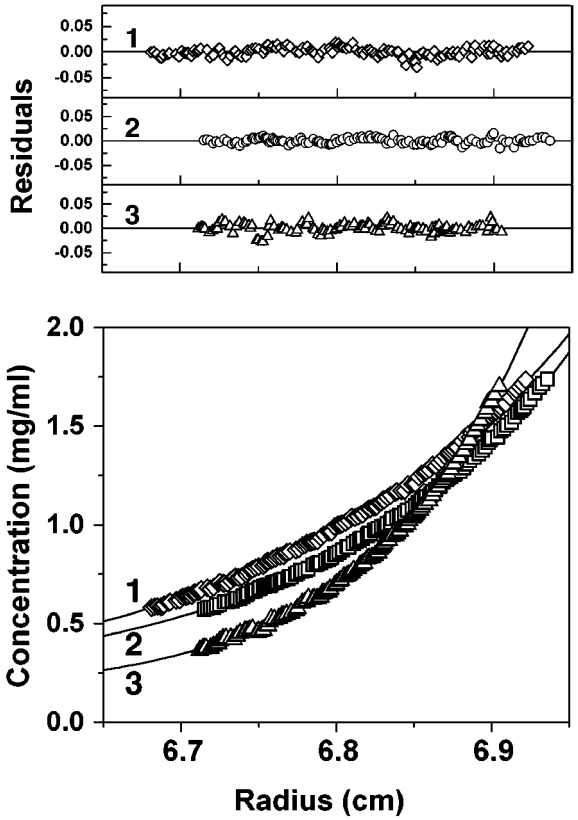

FIGURE 3: Sedimentation equilibrium analysis of the V_L domain at pH 2.35 (1), 3.95 (2), and 8.0 (3). The bottom panel shows the concentration vs radius plot. From these curves, the association (dimerization) constants (K_a) were calculated on the basis of the monomer−dimer equilibrium using the equation $K_a = [D]/[M]^2$, where [D] and [M] are molar concentrations of the dimeric and monomeric protein, respectively (*22*, *23*). The solid curves are theoretical ones, and the upper panel shows the residuals from the theoretical curves. Although it is difficult to interpret these profiles intuitively, the data with a larger inclination in the outer region result in a higher association constant. The K_a values were 4.8×10^5 M^{-1} at pH 8, 6.5×10^3 M^{-1} at pH 3.95, and 2.1×10^3 M^{-1} at pH 2.35. Using these K_a values and the above equation, the percentage of dimeric V_L calculated at the total V_L concentration of 0.45 mg/mL was 78% at pH 8, 16% at pH 3.95, and 6% at pH 2.35.

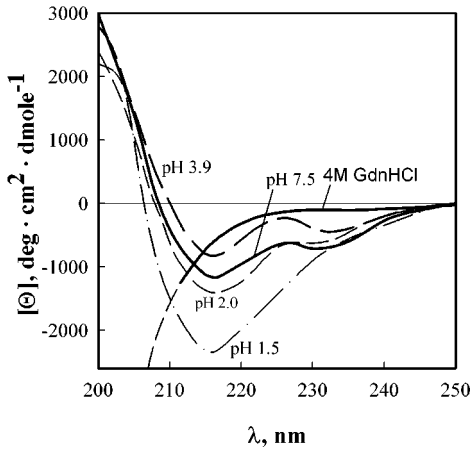

FIGURE 4: Formation of low-pH-induced partially unfolded conformations of the V_L domain as monitored by far-UV CD spectra.

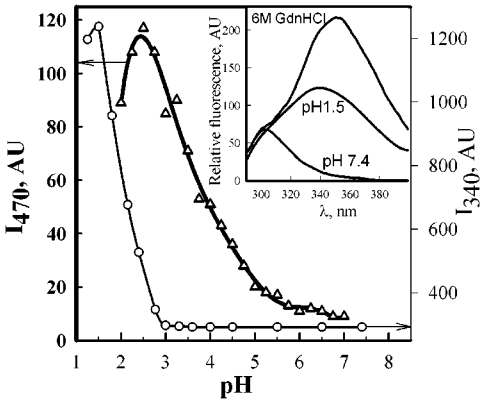

FIGURE 5: Partial pH-induced unfolding of the V_L domain as measured by the intrinsic protein fluorescence (○, right *Y* axis) and the fluorescence of bound ANS (△, left *Y* axis). To generate the ANS fluorescence spectra, the V_L domain was mixed with a fluorescent dye (see Materials and Methods) and the dye emission spectrum was monitored. The inset shows the intrinsic fluorescence of V_L under native conditions and at pH 1.5, and the spectrum of the GdnHCl-unfolded protein.

domains (*28*). All the results were analyzed satisfactorily on the basis of a monomer−dimer equilibrium mechanism to obtain the association constant (K_a). At neutral pH, a K_a value of 4.8×10^5 M^{-1} was obtained, and the V_L domain was predominantly dimeric. Association constants on the same order of magnitude [2.4×10^5 M^{-1} (*28*) and 1×10^5 M^{-1} (*29*)] were reported previously for human V_L domains of Bence Jones proteins.

On the basis of the association constant obtained for our V_L domain, the population of monomeric species at neutral pH was calculated to be ∼15% at the concentration of 1 mg/mL employed in our in vitro fibrillogenic studies. At pH 3.95, the pH value that provided reliable detection of fibrils after incubation for 3 days, the association constant was decreased to 6.5×10^3 M^{-1} and the population of monomeric species increased; at a V_L concentration of 1 mg/mL, the percentage of monomeric V_L was ∼27%. At strongly acidic pH (e.g., 2.35), the monomeric species dominated, with the population of dimeric V_L being as low as 6% at a V_L concentration of 0.45 mg/mL, while at the fibrillogenic concentration (1 mg/mL), the calculated dimeric fraction was ∼12%.

CD. The far-UV CD spectrum of the V_L domain (Figure 4) at pH 7.5 exhibited minima at 216 and 230 nm. While the minimum at 216 nm was typical for the β-sheet structure of an immunoglobulin domain, the minimum at 230 nm was attributed to contributions from aromatic interactions and, presumably, the disulfide bond. When the far-UV CD spectrum was measured as a function of pH, we observed a slight decrease in the CD intensity at pH ∼3.9. Then, the CD intensity increased markedly in magnitude below pH 2.0. A similar low-pH-induced increase in the negative ellipticity around 218 nm was observed previously at pH 2 for partially structured states of human amyloidogenic V_L domain SMA (*6*), mouse monoclonal IgG1 antibody (*30*), and rabbit IgG (*18*). However, the reported spectra exhibited substantial disordering of secondary structure judging from the shift of the minimum to a wavelength of <210 nm. In contrast, the spectrum of the mouse V_L domain at pH 1.5 exhibited a minimum at 216 nm, typical for the β-sheet structure. Furthermore, the spectrum at pH 1.5 was distinct from that of the GdnHCl-unfolded protein. The CD spectra indicated that our V_L domain retained a significant amount of nativelike secondary structure at pH 1.5 and was more ordered than the structures described above.

ANS Binding. ANS binding studies (Figure 5) were performed to investigate the presence of water-accessible hydrophobic surfaces in the intermediate states accumulated during acid denaturation. ANS binding species with a maximum at 470 nm appeared as early as pH ∼5.5, consistent with the highest fibrillogenic pH revealed with thioflavin T (pH 5.6, Figure 1). Intriguingly, the maximum level of ANS binding was observed at pH ∼3, lower than the maximal pH of amyloid fibril formation. Under strongly acidic conditions, the population of ANS binding species decreased, suggesting formation of a more substantially unfolded conformation with a decrease in hydrophobic surfaces. However, even at a pH as low as 2, the protein still demonstrated significant binding of ANS, suggesting that an intermediate with exposed hydrophobic surfaces was still present. This finding was consistent with our DSC data obtained at pH 2 (see below).

Tryptophan Fluorescence. The fluorescence spectrum of the V_L domain at pH 7.4, with excitation at 280 nm, exhibited an emission maximum at 305 nm with negligible intensity at ∼350 nm (Figure 5, inset). This showed that the fluorescence of a single and highly conserved Trp35 was strongly quenched by the intrachain disulfide bond located in spatial proximity (*3*, *30*, *31*). In the pH range between pH 7.5 and 3, the intrinsic fluorescence spectrum of the V_L domain (Figure 5) remained essentially unchanged. Between pH 3 and 1.5, the spectra revealed a prominent dequenching effect with the appearance of the emission band that can be attributed to the tryptophanyl fluorophore. This dequenching effect strongly suggested a partial loss of tertiary interactions, which resulted in removal of an internal quencher (presumably, the disulfide bond) from the vicinity of the Trp35 residue. The spectrum at pH 1.5 was, however, distinct with respect to both the intensity and maximal wavelength from that obtained for the protein after complete unfolding with 6 M GdnHCl, indicating that the unfolding was incomplete.

Although ANS fluorescence showed a transition curve starting at pH 5.5, the intrinsic fluorescence revealed a highly cooperative unfolding transition that occurred at strongly

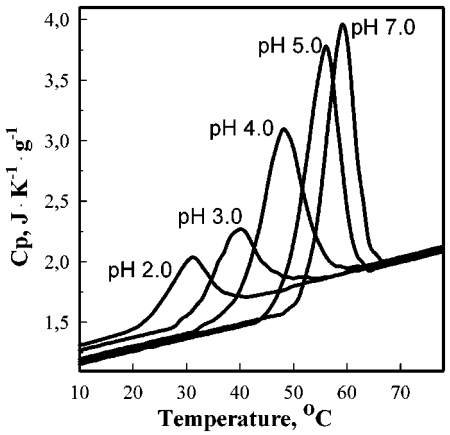

FIGURE 6: Characterization of partial pH-induced unfolding of the V_L domain by differential scanning calorimetry. Midpoint transition temperatures (T_m) and specific thermal unfolding enthalpies (Δh) were as follows: 59.5 °C and 16.3 J/g at pH 7.0, 56 °C and 15.9 J/g at pH 5, 48 °C and 13.0 J/g at pH 4.0, 39.4 °C and 7.5 J/g at pH 3.0, and 31 °C and 4.2 J/g at pH 2.0, respectively.

acidic pH. Taken together, these observations indicated the presence of a marginal structure that was destabilized between pH 3 and 7.5 and a more rigid structure that comprises Trp35 and undergoes highly cooperative denaturation below pH 3.

Differential Scanning Calorimetry. DSC (Figure 6) demonstrated that thermal unfolding of the V_L domain at pH 7 was accompanied by a prominent heat absorption peak and an increase in heat capacity, as generally observed for globular proteins. At pH 7.0, the midpoint transition temperature (T_m) and the specific transition enthalpy (Δh) were 59.5 °C and 16.3 J/g, respectively. The decrease in pH resulted in a decrease in the transition temperature and a concomitant decrease in the magnitude of the heat absorption peak, apparently similar to those observed for many small globular proteins. Furthermore, the heat capacity below the transition temperature was markedly increased, suggesting partial exposure of hydrophobic residues, consistent with our ANS binding studies.

However, because the observed decreases in T_m and Δh were accompanied by pH-dependent changes in the monomer−dimer equilibrium and the accumulation of intermediates, unambiguous quantitative analysis of the calorimetric data is not straightforward. Nonetheless, our DSC curve at a pH as low as 2 clearly demonstrated the heat absorption peak and the evident increase in heat capacity upon unfolding. This strongly suggested that the intermediate state present at pH 2.0 retains a compact structure with an internal hydrophobic core capable of a cooperative thermal unfolding transition.

NMR. The one-dimensional NMR spectra allowed us to discriminate between the denaturant-unfolded protein and the conformational states of the V_L domain obtained at pH 7.5, 4, and 2 (Figure 7). At pH 7.5, the NMR spectrum represented the pattern typical for a native protein. The resonance peaks were sharp, and the chemical shifts were well-resolved and dispersed throughout the whole field range. Whereas the NMR spectrum at pH 4.0 still exhibited the nativelike pattern, the spectrum at pH 2 was consistent with that of a partially structured state. This difference was clearly seen in upfield-shifted resonances and, in particular, in the low field between 9 and 7.5 ppm. At pH 2, the peak for methyl protons at 0.5 ppm was sharp and large, indicating that the methyl protons are flexible.

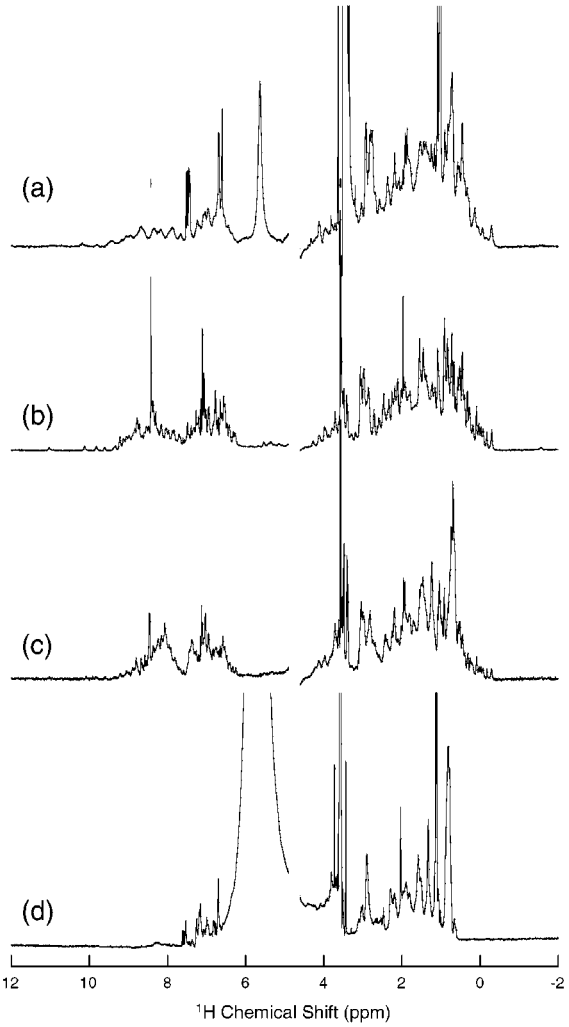

FIGURE 7: ^{1}H NMR spectra of the V_L conformational states induced by acidic pH or urea. One-dimensional NMR spectra were collected at 20 °C and a V_L concentration of 2 mg/mL at pH 7.5 (a), 4.0 (b), and 2.0 (c) and in 6 M urea at pH 2.0 (d).

The spectrum of the urea-denatured V_L domain was distinct from the spectra of both the native protein at pH 7.5 and the partially structured state at pH 2. The spectrum in the presence of 6 M urea displayed a significantly lower dispersion lacking the upfield-shifted methyl resonances, and the peaks were narrower in comparison with those observed for the native V_L domain or its partially structured states at pH 2.

DISCUSSION

The mouse V_L domain of the antiferritin antibody F11 does not produce fibrils under physiological conditions. However, we showed that partial unfolding of the V_L domain by decreasing pH yields genuine amyloid fibrils as evidenced by electron microscopy and supported by thioflavin T binding and apple-green birefringence after staining with Congo red. This is the first report of amyloid fibril formation of the mouse V_L domain.

To understand the relationship between the protein conformation and amyloid fibril formation, we analyzed the pH-

Table 1: Conformational Properties of the Mouse V_L Domain

property	I_2 that accumulates at pH 1.5	I_1 that accumulates at pH 3.0	native state at pH 7.5
amyloid fibril formation	+	++	−
monomer or dimer at 0.5 mg/mL	monomer	monomer	dimer
ANS binding	ND	++	−
ellipticity at 216 nm	−2200	−1200	−1300
tryptophan fluorescence	++	−	−
DSC peak	ND	+	+

induced unfolding transitions by various methods, including sedimentation equilibrium, ANS binding, far-UV CD, tryptophan fluorescence, DSC, and NMR. The results suggested the presence, at acidic pH, of at least two intermediate states that are distinct from both the native state present at neutral pH and the denaturant-unfolded state (Table 1).

Acidic Intermediates. The pH-induced unfolding process resulted in formation of at least two distinct conformations. First, partial unfolding when the pH is decreased from pH 7 to 3 yielded an unfolding intermediate (I_1) with a slightly distorted secondary structure and a significantly distorted tertiary conformation. The above conformational changes were revealed by CD, one-dimensional NMR, and ANS binding. The V_L dimer was destabilized by decreasing the pH, and the monomer is probably less stable than the dimer. This may explain the gradual transition observed by ANS binding between pH 6 and 4. The I_1 intermediate retains the hydrophobic core, as suggested by the clearly seen heat absorption peak on the DSC curves at pH 3 or 2. This was consistent with the observation that the intrinsic fluorescence spectrum of the above unfolding intermediate remained markedly quenched, indicating the nativelike local structure around the buried single tryptophan residue, Trp35.

The further and highly cooperative unfolding transition below pH 3 produced the second and more unfolded intermediate (I_2) that displayed more pronounced changes in the CD and NMR spectra as well as a decrease in ANS fluorescence. The distinctive feature of this more unfolded conformation was the remarkable dequenching of fluorescence emission for the Trp35 residue. The CD spectrum with a minimum at 216 nm indicated that even this second unfolding process did not, however, lead to complete unfolding of the β-sheet.

The two partially unfolded intermediates of the V_L domain met the criteria of a molten globule-like state. The molten globule states bind the hydrophobic fluorescent dye ANS and possess a significant amount of a distorted secondary structure, together with a destabilized tertiary structure. It should be noted that the definition of the molten globule state at present is not as strict as originally proposed, and it can accommodate a variety of compact denatured states with retention of nativelike secondary structures (*32*).

The V_L-comprising multidomain modules such as full-length immunoglobulins (*18*, *30*, *33*), their Fab fragments (*33*−*35*), and the Bence Jones protein IVA (*36*) have been analyzed using calorimetric and spectroscopic probes under low-pH conditions. However, the structural complexity of these modules appeared to be too high to allow definitive attribution of calorimetrically revealed transitions to constituent domains. The full-length monoclonal antibody of the mouse IgG1 subclass (*30*) and its Fab fragment (*35*) were shown to adopt, at pH 2−3, an alternatively folded state, the so-called A-state. This state constitutes a molten globule-like conformation with anomalously high thermal stability presumably conferred by interactions between partially folded domains. Dissociation of the Fab fragment into the individual light chain (V_L-C_L tandem) and the Fd fragment (V_H-C_H1 domains of the heavy chain) yielded another partially structured conformation distinct from the A-state (*35*).

The molten globule-like conformations of the mouse V_L domains observed here are, however, distinct from the alternatively folded A-state previously found for the mouse IgG1, IgG2a, and Fab fragments (*30*, *33*, *35*) as they do not reproduce a distinctive feature of the A-state, i.e., a paradoxical increase in the thermal stability in terms of T_m observed together with a marked decrease in the thermal unfolding enthalpy. Our results provided further evidence supporting the concept (*35*) that interaction between the immunoglobulin light and heavy chains is critical for folding of the A-state. Furthermore, our results argued that the first unfolding process that yields the less unfolded intermediate is accompanied by marked dissociation of the dimeric V_L domain into a monomeric species, and the monomer dominates under the conditions that provide more significant unfolding.

Amyloid Fibril Formation. It remains to be established whether the dissociation of subunit interactions contributes to the partial unfolding and/or amyloidogenic propensity of the V_L domain. Tryptophyl fluorescence (Figure 5, inset) and NMR (Figure 7) spectra at pH 4.0 suggested the nativelike structure of the monomers, while ANS binding (Figure 5) indicated that the dissociation is accompanied by partial unfolding exposing the hydrophobic surfaces. However, it is also possible that the dimer interface exposed upon dissociation constitutes the binding site for ANS, without denaturation of the native structure. The CD spectrum at pH 3.9 is too ambiguous to allow a definitive conclusion regarding conformational changes in comparison with that at pH 7.5 or 2.0. The amino acid residues involved in hydrogen bonding at the V_L-V_L subunit interface in our V_L dimer were Gln38 and Gln89, Tyr36, and Phe96 (*37*). In this regard, dissection of interactions between subunits by engineering the domain interface would be of interest with a view to analyzing the conformation and amyloidogenic properties of predominantly monomeric V_L mutants.

The next question to be addressed is which of the two intermediate states, I_1 or I_2, is responsible for amyloid fibril formation. The marked decrease in the initial rate of fibril formation below pH 4 (Figure 1) suggested that the less unfolded I_1 intermediate is a more reasonable candidate for the amyloidogenic precursor. However, our spectroscopic and calorimetric measurements cannot exclude the possibility that a small amount of the I_2 intermediate is populated at the most efficient fibrillogenic pH values (pH 3−4) where the I_1 state is the dominant molecular species. Besides the population of the amyloidogenic intermediate, other driving forces might contribute to the apparent decrease in V_L amyloidogenicity below pH 3. Therefore, from our data, we cannot unambiguously ascribe amyloidogenic properties to one or both of the above intermediate states.

In this context, the monomeric amyloidogenic intermediate of transthyretin was proposed to be more structured than its molten globule state (*10*). In contrast, Khurana et al. (*6*)

proposed that the relatively unfolded but compact intermediate I_U readily forms amyloid fibrils, whereas the nativelike I_N preferentially leads to amorphous aggregates. In the case of β_2-microglobulin, substantial unfolding is necessary to initiate the seed-dependent extension reaction (*11*). Thus, on the basis of the information available at present, the extent of unfolding necessary for amyloid fibril formation seems to depend on protein species.

ACKNOWLEDGMENT

We thank Miyo Sakai for the sedimentation equilibrium measurements.

REFERENCES

1. Ivanyi, B. (1990) *Arch. Pathol. Lab. Med. 114*, 986−987.
2. Hurle, M. R., Helms, L., Li, L., and Wetzel, R. (1994) *Proc. Natl. Acad. Sci. U.S.A. 91*, 5446−5450.
3. Helms, L., and Wetzel, R. (1995) *Protein Sci. 4*, 2073−2081.
4. Helms, L., and Wetzel, R. (1996) *J. Mol. Biol. 257*, 77−86.
5. Raffen, R., Dieckman, L. J., Szpunar, M., Wunschl, C., Pokkuluri, P. R., Dave, P., Stevens, P. W., Cai, X., Schiffer, M., and Stevens, F. (1999) *Protein Sci. 8*, 509−517.
6. Khurana, R., Gillespie, J. R., Talapatra, A., Minert, L. J., Ionescu-Zanetti, C., Millett, I., and Fink, A. L. (2001) *Biochemistry 40*, 3525−3535.
7. Rostagno, A., Vidal, R., Kaplan, B., Chuba, J., Kumar, A., Elliot, J. I., Frangione, B., Gallo, G., and Ghiso, J (1999) *Br. J. Haematol. 107*, 835−843.
8. Ionescu-Zanetti, C., Khurana, R., Gillespie, J. R., Petrick, J. S., Trabachino, L., Minert, L. J., Carter, S. A., and Fink, A. L. (1999) *Proc. Natl. Acad. Sci. U.S.A. 96*, 13175−13179.
9. Colon, W., and Kelly, J. W. (1992) *Biochemistry 31*, 8654−8660.
10. Kelly, J. W. (1996) *Curr. Opin. Struct. Biol. 6*, 11−17.
11. Naiki, H., Hashimoto, N., Suzuki, S., Kimura, H., Nakakuki, K., and Gejyo, F. (1997) *Amyloid 4*, 223−232.
12. Naiki, H., and Gejyo, F. (1999) *Methods Enzymol. 309*, 305−318.
13. McParland, V. J., Kad, N. M., Kalverda, A. P., Brown, A., Kirvin-Jones, P., Hunter, M. G., Sunde, M., and Radford, S. E. (2000) *Biochemistry 39*, 8735−8746.
14. Booth, D. R., Sunde, M., Bellotti, V., Robinson, C. V., Hutchinson, W. L., Fraser, P. E., Hawkins, P. N., Dobson, C. M., Radford, S. E., Blake, C. C. F., and Pepys, M. B. (1997) *Nature 385*, 787−793.
15. Solomon, A., Weiss, D. T., and Pepys, M. B. (1992) *Am. J. Pathol. 140*, 629−637.
16. Martsev, S. P., Vlasov, A. P., and Arosio, P. (1998) *Protein Eng. 11*, 377−381.
17. Martsev, S., Chumanevich, A., Vlasov, A., Dubnovitsky, A., Tsybovsky, Ya., Deyev, S., Cozzi, A., Arosio, P., and Kravchuk, Z. (2000) *Biochemistry 39*, 8047−8057.
18. Martsev, S. P., Kravchuk, Z. I., Vlasov, A. P., and Lyakhnovich, G. V. (1995) *FEBS Lett. 361*, 173−175.
19. Kravchuk, Z. I., Chumanevich, A. A., Vlasov, A. P., and Martsev, S. P. (1998) *J. Immunol. Methods 217*, 131−141.
20. Privalov, P. L., and Khechinashvili, N. N. (1974) *J. Mol. Biol. 86*, 665−684.
21. Privalov, P. L., and Potekhin, S. A. (1986) *Methods Enzymol. 131*, 4−51.
22. Laue, T. M. D. S. B., Ridgeway, T. M., and Pelleteir, S. L. (1992) in *Analytical Ultracentrifugation in Biochemistry and Polymer Science* (Harding, S. E., Rowe, A. J., and Horton, J. C., Eds.) pp 90−125, The Royal Society of Chemistry, Cambridge, England.
23. Teller, D. C., Horbett, T. A., Richards, E. G., and Schachman, H. K. (1969) *Ann. N.Y. Acad. Sci. 164*, 66−101.
24. Sakurai, K., Oobatake, M., and Goto, Y. (2001) *Protein Sci. 10*, 2325−2335.
25. Laemmli, U. K. (1970) *Nature 227*, 680−685.
26. Gill, S. C., and von Hippel, P. H. (1989) *Anal. Biochem. 182*, 319−326.
27. Naiki, H., Higuchi, K., Hosokawa, M., and Takeda, T. (1989) *Anal. Biochem. 177*, 244−249.
28. Raffen, R., Wilkins-Stevens, P., Boogaard, C., Schiffer, M., and Stevens, F. J. (1998) *Protein Eng. 11*, 303−309.
29. Azuma, T., Kobayashi, O., Goto, Y., and Hamaguchi, K. (1978) *J. Biochem. 83*, 1485−1492.
30. Buchner, J., Renner, M., Lilie, H., Hinz, H.-J., Jaenicke, R., Kiefhaber, T., and Rudolf, R. (1991) *Biochemistry 30*, 6922−6929.
31. Tsunenaga, M., Goto, Y., Kawata, Y., and Hamaguchi, K. (1987) *Biochemistry 26*, 6044−6051.
32. Arai, M., and Kuwajima, K. (2000) *Adv. Protein Chem. 53*, 209−282.
33. Welfe, K., Misselwitz, R., Hausdorf, G., Hohne, W., and Welfe, H. (1999) *Biochim. Biophys. Acta 1431*, 120−131.
34. Tischenko, V. M., Zav'yalov, V. P., Medgyesi, G. A., Potekhin, S. A., and Privalov, P. L. (1982) *Eur. J. Biochem. 126*, 517−521.
35. Lilie, H., and Buchner, J. (1995) *FEBS Lett. 362*, 43−46.
36. Zav'yalov, V. P., Troitsky, G. V., Khechinashvili, N. N., and Privalov, P. L. (1977) *Biochim. Biophys. Acta 492*, 102−111.
37. Nymalm, Y., Kravchuk, Z., Salminen, T., Chumanevich, A., Dubnovitsky, A., Kankare, J., Pentikäinen, O., Lehtonen, Y., Arosio, P., Martsev, S., and Johnson, M. (2001) (submitted for publication).

BI015894U